


Magnon-assisted photon-phonon conversion in the presence of structured environmentsShi-fan Qi  and Jun Jing **Zhejiang Province Key Laboratory of Quantum Technology and Device, Department of Physics, Zhejiang University, Hangzhou 310027, Zhejiang, China* (Received 11 November 2020; revised 26 January 2021; accepted 24 March 2021; published 7 April 2021)

Quantum conversion or interface is one of the most prominent protocols in quantum information processing and quantum state engineering. We propose a photon-phonon conversion protocol in a hybrid magnomechanical system comprising a microwave optical mode, a driven magnon mode, and a mechanical-vibrating mode, which has attracted much interest and is expected to become a building block of the future quantum information network due to its controllability in coupling strengths. The microwave photons in the optical cavity are coupled to the magnons by the Zeeman interaction, and the latter are coupled to the mechanical phonons by the magnetostrictive interaction. With a strong photon-magnon interaction and a strong driving on the magnon, an effective Hamiltonian is constructed to describe the conversion between photons and phonons near their resonant point. The cavity-magnon system can then play the role of quantum memory. Moreover, the faithfulness of the photon-phonon conversion is estimated in terms of fidelities for state evolution and state-independent transfer. The former is discussed in the Lindblad master equation, taking account of the leakages of photons, phonons, and magnons into consideration. The latter is derived by the Heisenberg-Langevin equation considering the non-Markovian noise from the structured environments for both optical and mechanical modes. The state-evolution fidelity is found to be robust to the weak leakage. The transfer fidelity can be maintained by the Ohmic and sub-Ohmic environments of the photons and is insensitive to the $1/f$ noise of the phonons. Our work thus provides an interesting application for the magnon system as a photon-phonon converter in the microwave regime.

DOI: [10.1103/PhysRevA.103.043704](https://doi.org/10.1103/PhysRevA.103.043704)**I. INTRODUCTION**

The cavity-magnon system is a rapidly developing mesoscopic platform for quantum information processing [1–4]. As an active topic of research, it has been theoretically investigated [5–8] and experimentally demonstrated [7,9–13] in the perspective of cavity quantum electrodynamics (cQED) during the past decade. Following the circuit-QED [14] systems and the semiconductor microcavities systems (such as quantum dots embedded in cavities [15,16]), the cavity-magnon system actually becomes an alternative candidate for exploiting the ubiquitous effects of cQED in the strong-coupling regime [17–19].

Typically, in a cavity-magnon system, a magnet-spin ensemble in a single-crystal yttrium iron garnet (YIG) sphere is loaded into a high- Q cavity. Down to the quantum level, it is found that the Kittel mode of the spin ensemble (the ground state) in the YIG sphere could be strongly coupled to the microwave photons in a cavity mode, and in the meantime the magnons are coupled to the phonons, describing the mechanical vibration of the same sphere (see the diagram in Fig. 1). Then a cavity-magnon system could be considered as a cavity-optomechanical system, taking inspiration from the cavity optomechanics, where the optical mode is *directly* coupled to the mechanical vibration of the movable mirror via radiation

pressure [20]. Significant progress regarding the mechanical vibration has been reported to demonstrate the quantum advantages, such as the phonon cooling in a non-Markovian environment [21], the quantum entanglement between mechanical elements and cavity modes [22,23], and the quantum state transfer between photon and phonon [24]. In light of displaying the quantum characteristics, it is interesting to apply original ideas in the existing hybrid quantum systems [20,25–28] to the cavity-magnomechanical system. For example, an implementation of the photon-magnon-phonon interaction was addressed in Ref. [29], based on which the photon-magnon-phonon entanglement in cavity magnomechanics was proposed in Ref. [30].

In terms of quantum conversion, protocols for light-matter interface and state transfer have been implemented with atomic systems under cavity QED [31,32]. The quantum state conversion between microwave and optical photons was proposed via an optoelectromechanical interface [33]. Optomechanical systems can also serve as light-matter interfaces, in which quantum information and quantum fluctuations originally encoded in an optical field can be reversibly mapped to a mechanical oscillator with a much smaller decay rate [34,35], by which the mechanical oscillator serves as a quantum network node [29,30] for information storage and processing [36]. In this work, we present a protocol for photon-phonon conversion in the cavity magnomechanical system [30] on account of the fundamental interest in the physical process, also exploiting the strong coupling for the

*jingjun@zju.edu.cn

magnon-photon and the magnon-phonon interactions and the negligible phonon decay rate. Note the phonon in the YIG sphere decays with a rate about 100 Hz [29], much smaller than its own frequency and that of the photons. In comparison to the direct photon-phonon interaction in the well-studied cavity optomechanical system, our proposal realizes indirect photon-phonon interaction with the same order of magnitude in a three-mode system. A more important advantage of the cavity-magnomechanical system [29] is its potential large-scale parametric implementation due to the fact that the single coupling strength between magnon and phonon can be tuned from 0 to 60 MHz by manipulating the direction of the bias fields.

The strong coupling inside a hybrid system opens a door to study the physics of virtual processes governed by the interaction Hamiltonian and leads to many interesting phenomena and applications in quantum engineering [17–19]. For example, the interesting Bell states, GHZ states [37], and NOON states [38] can be generated in the strongly coupled circuit-QED systems by virtue of the multiple-photon process. We find that the core idea in these general Rabi models [37–39] describing a single atomic system strongly coupled to a harmonic oscillator system can be used to construct an effective Hamiltonian describing the indirect coupling between photon and phonon at their resonant point via the virtual process of magnons. In particular, the effective coupling obtained by the second-order perturbation theory [38,39] supports a different conversion protocol between the mechanical oscillation and the microwave optical mode, resembling the conventional one in the optomechanical systems.

The rest part of this work is structured as following. In Sec. II, we introduce the hybrid quantum model and derive the effective Hamiltonian for the photon-phonon conversion mediated by the magnon mode. In Sec. III, the effective Hamiltonian is confirmed by comparison to the original Hamiltonian with respect to the effective coupling strength and is phenomenologically tested in terms of the state evolution under the leakage of photon, magnon, and phonon by a Lindblad master equation. In Sec. IV, a state-independent transfer fidelity via the effective Hamiltonian is derived through a microscopic analysis via the Heisenberg-Langevin equation. It is shown that our conversion protocol can be implemented with high fidelity under certain structured environments for the photon mode. We discuss the Kerr non-linearity of the magnon mode on the effective Hamiltonian and then summarize the whole work in Sec. V.

II. MODEL AND THE EFFECTIVE HAMILTONIAN

We consider a hybrid cavity magnon-mechanical system as shown in Fig. 1, which is constituted by cavity-mode photons, magnons, and phonons [30] down to the quantum level. The magnons are embodied by a collective motion of a large number of spins in a ferrimagnet, e.g., a YIG sphere. Then the cavity photons are coupled to magnons via the Zeeman interaction between the magnetic field of light and the magnetization of the magnet sphere. The coupling between magnons and phonons is mediated by the magnetostrictive interaction. In particular, the temporally varying magnetization induced by the magnon excitation inside the YIG sphere leads to

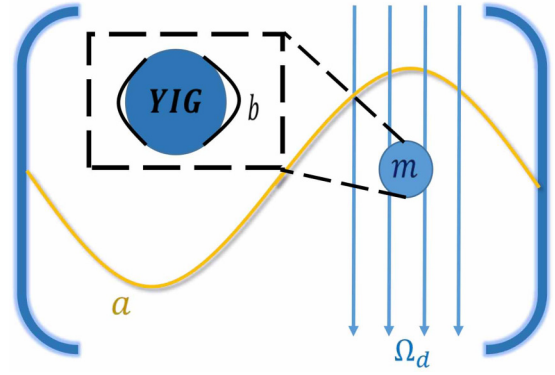


FIG. 1. Model diagram: a YIG sphere is placed inside a microwave cavity near the maximum magnetic field of the cavity mode and simultaneously in a uniform bias magnetic field, which establishes the magnon-photon coupling. The magnon mode is driven by a microwave source (with a magnitude Ω_d) to enhance the magnomechanical coupling.

the deformation of its geometrical structure, which forms the vibrational modes (phonons) of the sphere. The sphere size is considered to be much smaller than the wavelength of the microwave photons, such that the magnetic dipole interactions are isotropic and the effect of radiation pressure (proportional to the photon number $\langle a^\dagger a \rangle$) over the sphere is negligible. The system Hamiltonian thus reads ($\hbar \equiv 1$)

$$\begin{aligned}
 H_S = & \omega_a a^\dagger a + \omega_m m^\dagger m + \omega_b b^\dagger b \\
 & + i\Omega_d (m^\dagger e^{-i\omega_d t} - m e^{i\omega_d t}) \\
 & + g_{ma} (a m^\dagger + a^\dagger m) + g_{mb} m^\dagger m (b + b^\dagger). \quad (1)
 \end{aligned}$$

Here $a(a^\dagger)$, $m(m^\dagger)$, and $b(b^\dagger)$ are the annihilation (creation) operators of the photon, magnon, and phonon modes, respectively. ω_a , ω_m , and ω_b are their respective eigen frequencies. The Rabi frequency $\Omega_d = \gamma \sqrt{5N} B_0 / 4$ describes the coupling strength between the driving field with amplitude B_0 and frequency ω_d and the magnon mode, where γ is the gyromagnetic ratio and N is the number of spins [30]. The magnet-spin ensemble has a long coherent time [40] and strong dipole transitions for efficient coupling to the microwave photons. Thus, the magnon-microwave coupling strength g_{ma} can be larger than the dissipation rates of both cavity and magnon modes, κ_a and κ_m , entering into the strong-coupling regime, $g_{ma} > \kappa_a, \kappa_m$. To construct the Hamiltonian in Eq. (1), the photon-magnon interaction term is a result of linearizing magnetization using Holstein-Primakoff transformation, assuming that the magnetic field of light is of linear polarization and perpendicular to the static magnetization. We have employed the rotating-wave approximation, i.e., $g_{ma}(a + a^\dagger)(m + m^\dagger) \rightarrow g_{ma}(a m^\dagger + a^\dagger m)$, that is valid when $\omega_a, \omega_m \gg g_{ma}$ [29]. The single-magnon magnomechanical coupling strength g_{mb} is typically small, considering the large frequency mismatch between the magnon and the phonon modes, yet it can be compensated by a strong parametric drive Ω_d . In this case, the magnomechanical coupling is described by a radiation-pressure-like, dispersive interaction Hamiltonian $g_{mb} m^\dagger m (b + b^\dagger)$.

It is convenient to change the description of the microwave photon mode and the magnon mode by switching to a frame rotating at the driving frequency ω_d . Applying the unitary transformation $U = \exp(i\omega_d t a^\dagger a + i\omega_d t m^\dagger m)$ makes the driving terms time independent [20] and generates a rotating Hamiltonian $H'_S = U H U^\dagger - iU \partial U^\dagger / \partial t$ of the form

$$H'_S = \Delta_a a^\dagger a + \Delta_m m^\dagger m + \omega_b b^\dagger b + g_{mb} m^\dagger m (b + b^\dagger) + g_{ma} (a m^\dagger + a^\dagger m) + i\Omega_d (m^\dagger - m), \quad (2)$$

where $\Delta_a \equiv \omega_a - \omega_d$ and $\Delta_m \equiv \omega_m - \omega_d$. The magnon mode under driving is assumed to have a large expectation value $\langle m \rangle \equiv M \gg 1$, which allows us to linearize [20,41] the system dynamics by writing the operator $m = M + \delta m$ with δm describing the fluctuation of the magnon mode. The Hamiltonian H'_S turns out to be

$$H = H_0 + V, \\ H_0 = \Delta_a a^\dagger a + \Delta_m \delta m^\dagger \delta m + \omega_b b^\dagger b, \\ V = G(\delta m^\dagger + \delta m)(b + b^\dagger) + g(a \delta m^\dagger + a^\dagger \delta m), \quad (3)$$

where $g = g_{ma}$, and $G = M g_{mb}$ is the effective magnomechanical coupling strength. During the derivation over Eq. (3), all the linear terms have been omitted by an appropriate modulation over the detunings, since they indicate the presence of the average displacements. Then we only keep the quadratic interaction V [20]. For simplicity, we apply the convention $\delta m \rightarrow m$ in the following content.

To realize the photon-phonon conversion assisted by the magnon mode via the linearized approximate Hamiltonian in Eq. (3), generally one can extract an effective transition from the near-degenerate subspaces based on the standard perturbation theory with respect to the coupling strengths g and G . When the phonon frequency ω_b is near resonant with the detuning frequency Δ_a , and both of them are far off resonant from the detuning frequency Δ_m , i.e., $\omega_b \approx \Delta_a \gg g, G$ and $|\omega_b - \Delta_m| \gg g, G$, it is found that the tensor-product state $|n_a l_m k_b\rangle \equiv |n\rangle_a |l\rangle_m |k\rangle_b$ is near degenerate with $|(n-1)_a l_m (k+1)_b\rangle$. Here the subscripts a, m, b respectively represent the photon, magnon, and phonon modes, and n, l, k indicate their individual Fock states.

The indirect connection for any two eigenstates $|i\rangle$ and $|j\rangle$ of the unperturbed Hamiltonian H_0 can be constructed to the leading order by [37,39]

$$g_{\text{eff}} = \sum_{n \neq i, j} \frac{V_{jn} V_{ni}}{\omega_i - \omega_n}, \quad (4)$$

where $V_{nm} \equiv \langle n|V|m\rangle$ and ω_n is the eigenenergy of state $|n\rangle$, provided the interaction Hamiltonian V is regarded as a perturbation to H_0 .

A good approximation of the effective Hamiltonian describing the transition between arbitrary base pair $|nlk\rangle$ and $|(n-1)l(k+1)\rangle$ can be analytically obtained using the preceding second-order perturbation theory. It can be expressed in the form

$$H_{\text{eff}} = (\Delta_a + \epsilon_1) |nlk\rangle \langle nlk| + (\omega_b + \epsilon_2) |(n-1)l(k+1)\rangle \langle (n-1)l(k+1)| + g_{\text{eff}} (|nlk\rangle \langle (n-1)l(k+1)| + \text{H.c.}), \quad (5)$$

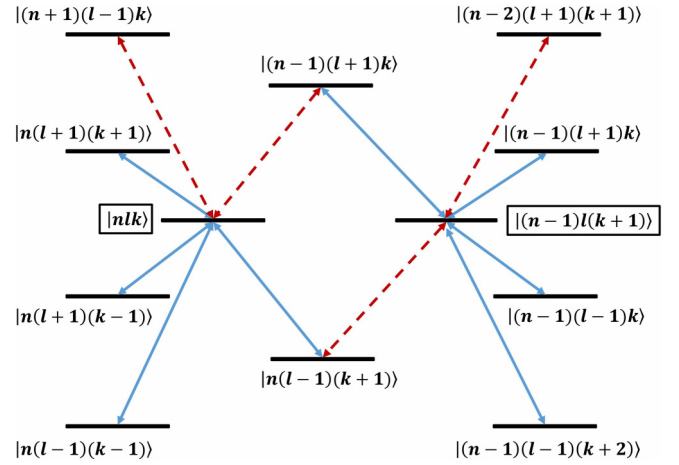


FIG. 2. All the second-order (leading-order) paths involving arbitrary base pair $|nlk\rangle \equiv |n\rangle_a |l\rangle_m |k\rangle_b$ and $|(n-1)l(k+1)\rangle$. Blue solid lines mark the transitions mediated by the photon-magnon coupling. Red long-dashed lines mark the transitions mediated by the magnon-phonon coupling.

where ϵ_1 and ϵ_2 are the energy shifts due to the effective coupling for the states $|nlk\rangle$ and $|(n-1)l(k+1)\rangle$, respectively, and g_{eff} is the effective coupling strength. These are three coefficients to be determined in this ansatz.

We first consider the energy shift ϵ_1 for the state $|nlk\rangle$. Summarizing all six paths from $|nlk\rangle$ and back to itself through an intermediate state (see Fig. 2), e.g., $|nlk\rangle \rightarrow |n(l-1)(k-1)\rangle \rightarrow |nlk\rangle$, one can obtain the second-order energy correction (shift) ϵ_1 according to Eq. (4)

$$\epsilon_1 = \frac{(n-l)g^2}{\Delta_a - \Delta_m} + \frac{(k-l)G^2}{\omega_b - \Delta_m} - \frac{(l+k+1)G^2}{\Delta_m + \omega_b}. \quad (6)$$

Similarly, the energy shift ϵ_2 for the state $|(n-1)l(k+1)\rangle$ is found to be

$$\epsilon_2 = \frac{(n-l-1)g^2}{\Delta_a - \Delta_m} + \frac{(k-l+1)G^2}{\omega_b - \Delta_m} - \frac{(m+l+2)G^2}{\Delta_m + \omega_b}. \quad (7)$$

Note an exact photon-phonon resonance facilitated by Eq. (5) allows a complete Rabi oscillation between arbitrary $|nlk\rangle$ and $|(n-1)l(k+1)\rangle$, which requires that the first two terms in Eq. (5) constitute the identity operator in the relevant subspace. Thus, $\Delta_a + \epsilon_1 = \omega_b + \epsilon_2$. Assuming the distance between Δ_a and ω_b is δ , one can then have

$$\delta \equiv \Delta_a - \omega_b = \epsilon_2 - \epsilon_1 \\ = \frac{G^2}{\omega_b - \Delta_m} - \frac{g^2}{\Delta_a - \Delta_m} - \frac{G^2}{\omega_b + \Delta_m} \\ = \frac{G^2 - g^2}{\omega_b - \Delta_m} - \frac{G^2}{\omega_b + \Delta_m} - \frac{g^2}{(\omega_b - \Delta_m)^2} \delta + O(\delta^2) \\ = A - B\delta + O(\delta^2), \quad (8)$$

where $A \equiv (G^2 - g^2)/(\omega_b - \Delta_m) - G^2/(\omega_b + \Delta_m)$, $B \equiv g^2/(\omega_b - \Delta_m)^2$, and $O(\delta^2)$ represents all the higher orders of δ from the first order in Taylor expansion. Then δ is consistently solved as $\delta = A/(1+B)$ up to the second-order correction. Note $B \approx O(g^2/|\omega_b - \Delta_m|^2)$, so that up to the second order

of the coupling strengths g or G , we have

$$\delta = \frac{G^2 - g^2}{\omega_b - \Delta_m} - \frac{G^2}{\omega_b + \Delta_m}. \quad (9)$$

Note δ is a Fock-state-independent coefficient in comparison to both ϵ_1 and ϵ_2 .

Next, we consider the contribution from the two paths connecting $|nlk\rangle$ and $|(n-1)l(k+1)\rangle$ in Fig. 2, i.e., $|nlk\rangle \rightarrow |(n-1)(l+1)k\rangle \rightarrow |(n-1)l(k+1)\rangle$ and $|nlk\rangle \rightarrow |n(l-1)(k+1)\rangle \rightarrow |(n-1)l(k+1)\rangle$, to their effective coupling strength. By virtue of Eq. (4), one can have

$$\begin{aligned} g_{\text{eff}} &= \frac{(l+1)\sqrt{n(k+1)}Gg}{\Delta_a - \Delta_m} - \frac{l\sqrt{n(k+1)}Gg}{\omega_b - \Delta_m} \\ &= \frac{(l+1)\sqrt{n(k+1)}Gg}{\omega_b - \Delta_m} \left[1 - \frac{\delta}{\omega_b - \Delta_m} + O(\delta^2) \right] \\ &\quad - \frac{l\sqrt{n(k+1)}Gg}{\omega_b - \Delta_m} \\ &= \sqrt{n(k+1)} \frac{Gg}{\omega_b - \Delta_m}, \end{aligned} \quad (10)$$

up to the second order of the coupling strengths g or G . Eventually, the effective Hamiltonian in Eq. (5) can be written as

$$\begin{aligned} H_{\text{eff}}^{(nk)} &= g_{\text{eff}}(|nlk\rangle\langle(n-1)l(k+1)| + \text{H.c.}) \\ &= g_{\text{eff}}(|nk\rangle\langle(n-1)(k+1)| + \text{H.c.}) \otimes |l\rangle\langle l|. \end{aligned} \quad (11)$$

The effective Hamiltonian extended to the whole Hilbert space of photon and phonon is therefore found to be

$$H_{\text{eff}} = \tilde{G}(ab^\dagger + ba^\dagger). \quad (12)$$

Here

$$\tilde{G} = \frac{Gg}{\omega_b - \Delta_m} \quad (13)$$

is the effective coupling strength of the two modes, which is in the same order as the deviation δ of the avoided level-crossing point from ω_b . More importantly, both \tilde{G} and δ are Fock state independent and robust to the variation in the magnon occupation number, which is the key to a generic conversion rather than the state transfer in special subspaces. It should be remarked that the same effective Hamiltonian could also be obtained by adiabatic elimination [42–44] in analog hybrid systems. The adiabatic-elimination technique forces the steady value of the fast variables into the dynamical equation to inversely obtain the effective Hamiltonian and then calculate the system shift δ and the effective coupling strength g_{eff} through some optimization procedure in the interested subspace, while the preceding treatment provides an alternative bottom-up approach to first derive these parameters and then obtain the effective Hamiltonian.

The effective Hamiltonian in Eq. (12) is conserved in the excitation number, so that it can be written in a block-diagonal matrix formation on the Fock-state basis. For example, if we focus on the single-exciton subspace $\{|001\rangle \equiv |0\rangle_a|0\rangle_m|1\rangle_b, |100\rangle\}$ in which the magnon remains at the

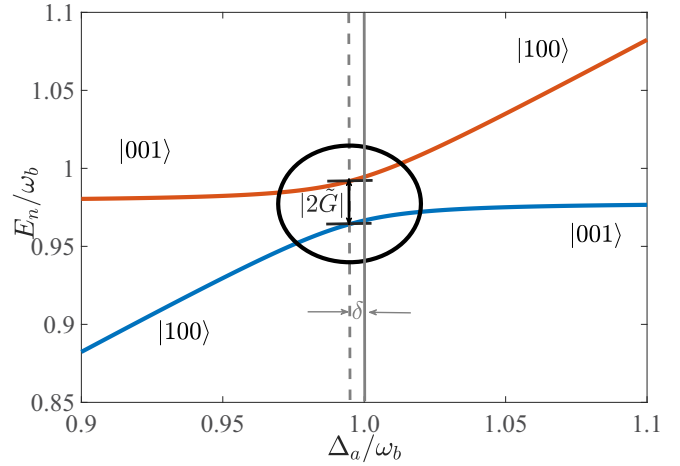


FIG. 3. Normalized energy-level diagram and avoided level crossing for the photon-phonon conversion in a single-exciton subspace, which are plotted as a function of the detuning frequency Δ_a/ω_b . Apparently the interactions in the system shift the avoided level crossing point from $\Delta_a/\omega_b = 1$ by δ , as given by Eq. (9). Here we fix $\Delta_m = 1.7\omega_b$ and $g = G = 0.1\omega_b$.

ground state, then we can have an X gate:

$$H_{\text{eff}}^{(1)} = \begin{bmatrix} 0 & \tilde{G} \\ \tilde{G} & 0 \end{bmatrix} = \tilde{G}\sigma_x. \quad (14)$$

We plot the associated energy levels in Fig. 3, where the eigenvalues $\{E_n\}$ and the eigenstates of the Hamiltonian in Eq. (3) are obtained by the standard numerical diagonalization method in a truncated Hilbert space. An avoided level crossing (distinguished in the dark circle) presents between two eigenstates of the original Hamiltonian in Eq. (3), when the detuning frequency of photon Δ_a approaches (but not exactly equals) the frequency of phonon ω_b . The mutual interaction between the photon and the magnon and that between the magnon and the phonon induce a negative shift from $\Delta_a = \omega_b$. Here we choose $\Delta_m = 1.7\omega_b$ to avoid unnecessary exciting of the magnon mode. When the system is prepared as $|100\rangle$, it can be converted to $|001\rangle$ via a half-Rabi oscillation determined by $H_{\text{eff}}^{(1)}$ after a duration $\pi/|2\tilde{G}|$.

The effective Hamiltonian in the double-exciton subspace spanned by $\{|002\rangle, |101\rangle, |200\rangle\}$, where the magnon remains at the ground mode, can be written as

$$H_{\text{eff}}^{(2)} = \begin{bmatrix} 0 & \sqrt{2}\tilde{G} & 0 \\ \sqrt{2}\tilde{G} & 0 & \sqrt{2}\tilde{G} \\ 0 & \sqrt{2}\tilde{G} & 0 \end{bmatrix}, \quad (15)$$

whose eigenstructure is found to be

$$\begin{aligned} E_1 &= \sqrt{2}\tilde{G}, & |\Psi_1\rangle &= \frac{|002\rangle + |200\rangle}{2} + \frac{|101\rangle}{\sqrt{2}}, \\ E_2 &= -\sqrt{2}\tilde{G}, & |\Psi_2\rangle &= \frac{|002\rangle + |200\rangle}{2} - \frac{|101\rangle}{\sqrt{2}}, \\ E_3 &= 0, & |\Psi_3\rangle &= \frac{|002\rangle - |200\rangle}{\sqrt{2}}, \end{aligned} \quad (16)$$

and the time-evolution operator reads

$$U(t) = \frac{1}{2} \begin{bmatrix} c+1 & -s\sqrt{2}i & c-1 \\ -s\sqrt{2}i & c & -s\sqrt{2}i \\ c-1 & -s\sqrt{2}i & c+1 \end{bmatrix} \quad (17)$$

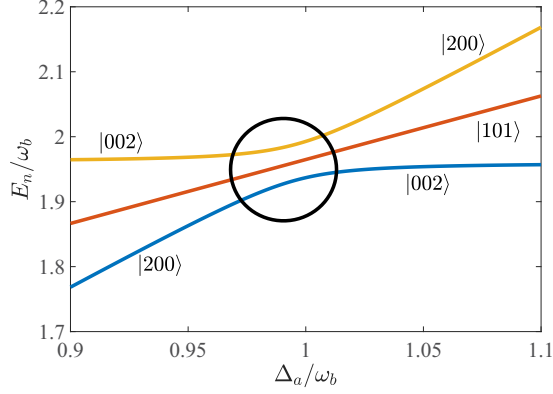


FIG. 4. Normalized energy-level diagram and avoided level crossing in a double-exciton subspace, which are plotted as a function of the detuning frequency Δ_a/ω_b . Here we fix $\Delta_m = 1.7\omega_b$ and $g = G = 0.1\omega_b$.

with $c \equiv \cos(2\tilde{G}t)$ and $s \equiv \sin(2\tilde{G}t)$. The energy diagram and the avoided level crossing between $|200\rangle$ and $|002\rangle$ are plotted in Fig. 4. The conversion time is still $\pi/|2\tilde{G}|$. In addition, it is interesting to observe that the last eigenstate $|\Psi_3\rangle$ is a dark state in this specific case. The vanishing eigenvalue implies that this eigenstate will remain intact during the time evolution.

More versatile physics can be exploited in the subspace with more excitons, in which the magnon always stays as the vacuum state. For a fixed total number of photon and phonon N , the effective Hamiltonian in Eq. (12) in the subspace spanned by $\{|N00\rangle, |(N-1)01\rangle, \dots, |10(N-1)\rangle, |00N\rangle\}$ can be expressed by

$$H_{\text{eff}}^{(N)} = \tilde{G} \begin{bmatrix} 0 & L_1 & 0 & \cdot & 0 \\ L_1 & 0 & L_2 & \cdot & 0 \\ 0 & L_2 & 0 & \cdot & 0 \\ \cdot & \cdot & \cdot & \cdot & \cdot \\ \cdot & \cdot & \cdot & \cdot & L_{N-1} \\ 0 & 0 & 0 & L_{N-1} & 0 \end{bmatrix}, \quad (18)$$

where $L_n = \sqrt{n(N-n)}$. It is interesting to be identical to the matrix representation of the Hamiltonian $H = 2\tilde{G}S_x$, where S_x is the angular momentum operator for a fictitious particle with spin $S = (N-1)/2$. The Hamiltonian $H_{\text{eff}}^{(N)}$ also describes an open-end spin chain governed by the site-dependent nearest-neighbor interactions [45]

$$H_{\text{spin}} = \sum_n \frac{\tilde{G}L_n}{2} (\sigma_n^x \sigma_{n+1}^x + \sigma_n^y \sigma_{n+1}^y), \quad (19)$$

which is used to realize a perfect state transfer through the chain. If the initial state is prepared as $|N00\rangle$, then the probability amplitude for state transfer is

$$A(t) = \langle 00N | \exp(-i2\tilde{G}S_x t) | N00 \rangle = [-i \sin(\tilde{G}t)]^{N-1}. \quad (20)$$

Therefore, the perfect conversion about a quantum state between photon and phonon is accomplished in a constant time $\pi/|2\tilde{G}|$, irrespective to the exciton number or the particular subspace. Ideally, any superposed state of the photon can be converted into the phonon mode through the evolution time $\pi/|2\tilde{G}|$.

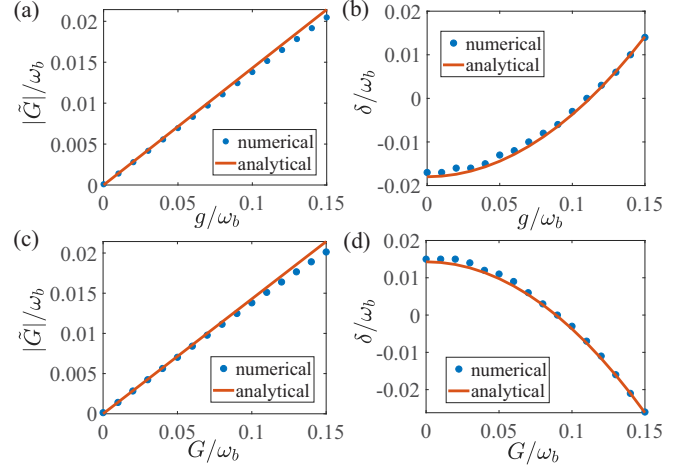


FIG. 5. [(a), (c)] Comparison between the numerically calculated normalized effective coupling strength $|\tilde{G}|/\omega_b$ (blue dots) and the corresponding analytical results in Eq. (3) from the second-order perturbation theory (orange solid lines) as functions of g/ω_b and G/ω_b , respectively; [(b), (d)] comparison between the numerically calculated normalized energy shift δ/ω_b (blue dots) and the corresponding analytical results in Eq. (9) (orange solid lines) as functions of g/ω_b and G/ω_b , respectively. For panels (a) and (b), $G = 0.1\omega_b$, and for panels (c) and (d), $g = 0.1\omega_b$. Here we fix $\Delta_m = 1.7\omega_b$.

III. THE APPLICATION RANGE OF THE EFFECTIVE HAMILTONIAN

We first check the applicability range of the effective Hamiltonian in Eq. (12) in terms of the coupling strength. It can be estimated or constrained by comparing the numerical results obtained from the original Hamiltonian in Eq. (3) for the full Hilbert space and the analytical results obtained via the perturbative derivation for the reduced subspace. The energy splitting $|\tilde{G}|$ of the two eigenstates at the avoided level-crossing point (see Fig. 3 in the single-exciton case) is presented in Figs. 5(a) and 5(c) as a function of the original coupling strengths g and G in the interaction Hamiltonian, respectively. The result given by the analytical expression in Eq. (13) is compared to that evaluated by the numerical simulation over the whole Hilbert space. It is found that the effective coupling strength $|\tilde{G}|$ is valid until $g/\omega_b \simeq 0.1$ and $G/\omega_b \simeq 0.1$. For a larger g or G , higher order contributions have to be included to capture the whole effect from the interaction Hamiltonian on modifying the eigenstructure of the bare system. However, an apparent yet still small deviation δ can be observed when either g or G is enhanced to $0.15\omega_b$. The effective Hamiltonian in Eq. (12) could therefore be used to investigate the strong-coupling regime.

Similarly, the energy shift δ in Eq. (9) can also be justified by Figs. 5(b) and 5(d). We check the same range of g and G as in Figs. 5(a) and 5(c). It is shown that the analytical results do match with the numerical ones, at least when the normalized photon-magnon interaction strength $g/\omega_b \leq 0.15$ or phonon-magnon coupling strength $G/\omega_b \leq 0.15$.

Next we take the open-quantum-system framework to further test the effective Hamiltonian in Eq. (12) in terms of the state-evolution fidelity. Under the standard assumptions (Markovian approximation, factorization of the system-

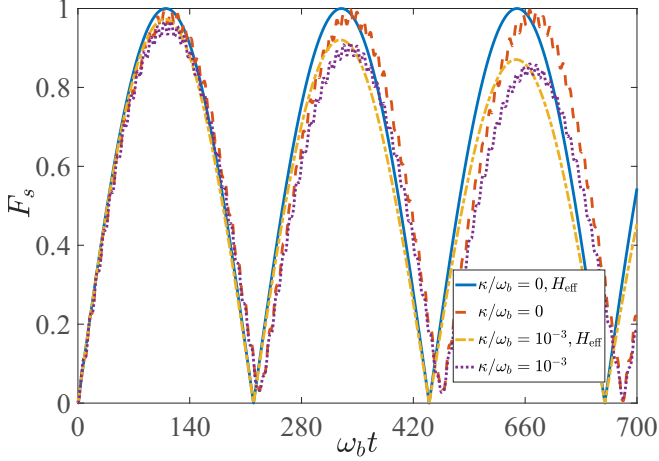


FIG. 6. Time evolution of the state fidelity by the master equations (21) and (23) to show the transfer between the initial state $|100\rangle$ and the target state $|001\rangle$. Here we fixed $\Delta_m = 1.7\omega_b$ and $g = G = 0.1\omega_b$.

environment density matrix, structure-free environment at the vacuum state), one can arrive at the Lindblad master equation for the density matrix of the interested hybrid system,

$$\begin{aligned} \dot{\rho}(t) = & -i[H, \rho(t)] + \kappa_a \mathcal{L}[a]\rho(t) \\ & + \kappa_m \mathcal{L}[m]\rho(t) + \gamma_b \mathcal{L}[b]\rho(t). \end{aligned} \quad (21)$$

Here H is the full Hamiltonian of the system given in Eq. (3), κ_a , κ_m , and γ_b are the relaxation rates for cavity mode, magnon, and phonon, respectively, and the superoperator $\mathcal{L}[O]$, $O = a, m, b$, is defined as

$$\mathcal{L}[O]\rho \equiv \frac{1}{2}(2O\rho O^\dagger - O^\dagger O\rho - \rho O^\dagger O). \quad (22)$$

For the effective model constituted by the photon and the phonon in Eq. (12), the Lindblad equation in the reduced subspace is written as

$$\dot{\rho}(t) = -i[H_{\text{eff}}, \rho(t)] + \kappa_a \mathcal{L}[a]\rho(t) + \gamma_b \mathcal{L}[b]\rho(t). \quad (23)$$

To simplify the discussion but with no loss of generality, we assume the decay rates of the photon and the magnon are the same $\kappa_a = \kappa_m = \kappa$, and set the decay rate of phonon $\gamma_b = 10^{-2}\kappa$ regarding that the decoherence rates of phonon are much smaller than that of cavity-mode or magnon [30].

Then one can numerically calculate the state fidelity $F_s = \sqrt{\langle \phi | \rho | \phi \rangle}$, where $|\phi\rangle$ is the target state, under either Eq. (21) or Eq. (23). The distinction between the results from different master equation measures both the validity of the effective Hamiltonian and the robustness of our photon-phonon conversion protocol. In Fig. 6, we plot the state-fidelity dynamics under different decoherence rates when the initial state and the target state are chosen as $|001\rangle$ and $|\phi\rangle = |100\rangle$, respectively. The blue solid line and the yellow dot-dashed line are the results from Eq. (23) using the effective Hamiltonian, and the orange dashed line and the purple dotted line are those from Eq. (21) using the full Hamiltonian. It is found that the results using the full Hamiltonian have a slightly longer period than those using the effective Hamiltonian in time evolution, yet they match almost with each other at least for the first two or three periods of Rabi oscillation. In the case

of no decoherence, the state fidelity achieves over 0.97 by the full Hamiltonian. With the Markovian decoherence rate $\kappa = 10^{-3}\omega_b$, both master equations produce the desired target state with a fidelity over 0.90 for photon-phonon conversion during the first period and maintain the target state with a fidelity about 0.85 during the third period.

IV. THE TRANSFER FIDELITY UNDER THE STRUCTURED ENVIRONMENTS

The phenomenological analysis on the Markovian errors on the state fidelity depends on the choice of the initial state and the target state during the photon-phonon conversion. It is indispensable to discuss the relationship between the transfer fidelity by the effective Hamiltonian that is independent of the state and the non-Markovian errors that are ubiquitous in almost all of the solid-state systems. In this section, we investigate the effect from the structured environment using the non-Markovian Heisenberg-Langevin equation [20,24], assuming that in a microscopic way the system is coupled to its environment consisting of a collection of independent harmonic oscillators. The total Hamiltonian reads

$$H_{\text{tot}} = H_{\text{eff}} + H_E + H_I. \quad (24)$$

Here the environmental Hamiltonian for the photon-phonon system reads

$$H_E = \sum_k \omega_k a_k^\dagger a_k + \sum_j \Omega_j b_j^\dagger b_j, \quad (25)$$

where ω_k and Ω_j are the reservoir frequency for the k th optical and the j th mechanical modes respectively. The two reservoirs are assumed to be uncorrelated. The interaction between the system and the environment can then be described by

$$H_I = \sum_k g_k (a_k^\dagger a + a^\dagger a_k) + \sum_j f_j (b_j^\dagger b + b^\dagger b_j), \quad (26)$$

where g_k and f_j are the respective system-reservoir coupling strengths for the optical mode and the mechanical mode [46] and supposed to be real numbers for simplicity. Here the interaction Hamiltonian is written in a form under the rotating-wave approximation, which is valid when the coupling strength is much smaller than the resonant frequency of the system, i.e., $g_k, f_j \ll \omega_b, \Delta_a$.

With the effective Hamiltonian for the system part in Eq. (12) and the interaction Hamiltonian in Eq. (26), one can write down the Heisenberg-Langevin equations in the rotating frame with respect to the environmental Hamiltonian in Eq. (25),

$$\dot{O}(t) = -iCO(t) - \int_0^t d\tau \bar{F}(t-\tau)O(\tau) + \epsilon_{\text{in}}(t). \quad (27)$$

Here the time-evolution operator for the system modes is $O(t) = (a(t), b(t))^T$ and the input noise operator is $\epsilon_{\text{in}}(t) = (a_{\text{in}}(t), b_{\text{in}}(t))^T$, where $a_{\text{in}} \equiv -i \sum_k g_k e^{-i\omega_k t} a_k(0)$ and $b_{\text{in}} \equiv -i \sum_j f_j e^{-i\Omega_j t} b_j(0)$ depend on the initial condition of the environment. The thermal average occupation numbers in the particular modes of the two reservoirs are $\bar{n}_a(\omega_k) \equiv \langle a_k^\dagger(0)a_k(0) \rangle = 1/[\exp(\hbar\omega_k/k_B T_a) - 1]\delta_{kk'}$ and $\bar{n}_b(\omega_j) \equiv \langle b_j^\dagger(0)b_j(0) \rangle = 1/[\exp(\hbar\omega_j/k_B T_b) - 1]\delta_{jj'}$,

respectively. The coefficient matrixes C and $\bar{F}(t)$ are given by

$$C = \begin{pmatrix} 0 & \tilde{G} \\ \tilde{G} & 0 \end{pmatrix}, \quad \bar{F}(t) = \begin{pmatrix} f_a(t) & 0 \\ 0 & f_b(t) \end{pmatrix}, \quad (28)$$

respectively, where $f_a(t) \equiv \sum_k g_k^2 e^{-i\omega_k t}$ and $f_b(t) \equiv \sum_j f_j^2 e^{-i\Omega_j t}$ are the nonlocal time correlation functions. We can rewrite the correlation functions by introducing the spectral density functions

$$f_x(t) = \int d\omega J_x(\omega) e^{-i\omega t}, \quad x = a, b \quad (29)$$

for the optical and the mechanical environments, respectively. The environment for the cavity mode is generally of an Ohmic-like spectrum, i.e., $J_a(\omega) = \eta\omega(\omega/\omega_0)^{s-1}e^{-\omega/\omega_0}$, where η is a dimensionless coupling strength between system and environment, and ω_0 is a high-frequency cutoff [47]. The parameter s classifies the environment as sub-Ohmic ($0 < s < 1$), Ohmic ($s = 1$), or super-Ohmic ($s > 1$). For the phonon mode in the YIG sphere, the solid-state environment is assumed to be a $1/f$ -like spectrum, similar to that for the optomechanical system recently measured in experiments. We therefore use the spectral density function $J_b(\omega) = c\omega^k$, where the coupling coefficient $c > 0$, k is a negative number around -1 [48], and the bandwidth in this work is chosen as $\omega \in (0.1\omega_b, 2\omega_b)$.

Formally, Eq. (27) can be solved by assuming $O(t) = \mathcal{U}(t)O(0) + \mathcal{V}(t)$, where $\mathcal{U}(t)$ is a 2×2 coefficient matrix ($\mathcal{U}_{11}(t), \mathcal{U}_{12}(t); \mathcal{U}_{21}(t), \mathcal{U}_{22}(t)$) as a function of time, and $\mathcal{V}(t)$ is a vector of operators ($\mathcal{V}_1(t), \mathcal{V}_2(t)$)^T related to the nonequilibrium Green's functions of the system. These Green's functions obey the following Dyson equations:

$$\begin{aligned} \dot{\mathcal{U}}(t) &= -iC\mathcal{U}(t) - \int_0^t d\tau \bar{F}(t-\tau)\mathcal{U}(\tau), \\ \dot{\mathcal{V}}(t) &= -iC\mathcal{V}(t) - \int_0^t d\tau \bar{F}(t-\tau)\mathcal{V}(\tau) + \epsilon_{\text{in}}(t). \end{aligned} \quad (30)$$

Considering the initial conditions $\mathcal{U}(0) = \mathcal{I}$ and $\mathcal{V}(0) = 0$, one can formally have

$$\mathcal{V}(t) = \int_0^t d\tau \mathcal{U}(t-\tau)\epsilon_{\text{in}}(\tau). \quad (31)$$

With the solution about $\mathcal{U}(t)$, the dynamical evolution of $b(t)$ is written as

$$b(t) = \mathcal{U}_{21}(t)a(0) + \mathcal{U}_{22}(t)b(0) + \mathcal{V}_2(t). \quad (32)$$

Then the expectation value of the phonon number $\langle b^\dagger(t)b(t) \rangle$ can be evaluated by

$$\begin{aligned} \langle b^\dagger(t)b(t) \rangle &= |\mathcal{U}_{21}(t)|^2 \langle a^\dagger(0)a(0) \rangle + |\mathcal{U}_{22}(t)|^2 \langle b^\dagger(0)b(0) \rangle \\ &\quad + \langle \mathcal{V}_2^\dagger(t)\mathcal{V}_2(t) \rangle. \end{aligned} \quad (33)$$

The first term on the right-hand side of Eq. (33) is proportional to the initial average number of photon $\langle a^\dagger(0)a(0) \rangle$. The second term is proportional to the initial average number of phonon $\langle b^\dagger(0)b(0) \rangle$, whose contribution could be reduced by precooled the mechanical oscillator to the ground state. As

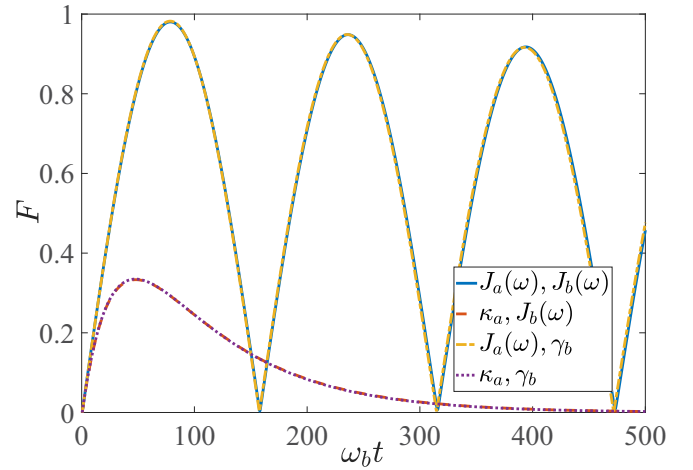


FIG. 7. The time evolution of the transfer fidelity under various environments. The parameters for the structured environments are chosen as $|\tilde{G}| = 0.02\omega_b$, $\eta = 1 \times 10^{-4}\omega_b$, $\omega_0 = 5\omega_b$, $s = 1$, $c = 1 \times 10^{-4}\omega_b$, and $k = -1$. For the Markovian environments, the decay rates κ_a and γ_b are obtained by the Weisskopf-Wigner theory.

for the last term, one can express it by

$$\begin{aligned} \langle \mathcal{V}_2^\dagger \mathcal{V}_2 \rangle &= \int \frac{d\omega}{2\pi} J_a(\omega) \bar{n}_a(\omega) \left| \int_0^t \mathcal{U}_{21}(t-\tau) e^{-i\omega\tau} \right|^2 \\ &\quad + \int \frac{d\omega}{2\pi} J_b(\omega) \bar{n}_b(\omega) \left| \int_0^t \mathcal{U}_{22}(t-\tau) e^{-i\omega\tau} \right|^2. \end{aligned} \quad (34)$$

Assume the environmental temperature for the photon mode $T_a \approx 0$ and the bandwidth of the spectral density for the mechanical environment is sufficiently narrow around the resonant frequency, the average value $\langle \mathcal{V}_2^\dagger \mathcal{V}_2 \rangle$ is upper bounded by $\bar{n}_b(\omega_b) [\mathcal{V}_2, \mathcal{V}_2^\dagger]$ due to the fact that

$$\begin{aligned} [\mathcal{V}_2, \mathcal{V}_2^\dagger] &= \int \frac{d\omega}{2\pi} J_a(\omega) \left| \int_0^t \mathcal{U}_{21}(t-\tau) e^{-i\omega\tau} \right|^2 \\ &\quad + \int \frac{d\omega}{2\pi} J_b(\omega) \left| \int_0^t \mathcal{U}_{22}(t-\tau) e^{-i\omega\tau} \right|^2. \end{aligned} \quad (35)$$

Also note the commutation relation $[b(t), b^\dagger(t)] = 1$ holds for any moment t , which renders

$$|\mathcal{U}_{21}|^2 + |\mathcal{U}_{22}|^2 + [\mathcal{V}_2, \mathcal{V}_2^\dagger] = 1. \quad (36)$$

Apparently $[\mathcal{V}_2, \mathcal{V}_2^\dagger] \geq 0$. It means that under a low-temperature T_b , both $|\mathcal{U}_{22}|$ and $\langle \mathcal{V}_2^\dagger \mathcal{V}_2 \rangle$ are close to zero when $|\mathcal{U}_{21}| \approx 1$. We therefore understand that the transfer fidelity F from photon to phonon can be quantified by $|\mathcal{U}_{21}(t)|$ [24] using the numerical solution of Eq. (30). Note this fidelity is obtained in the Heisenberg picture. It is then independent of the initial and target states.

We first comparing the noise effects on F from various combinations of the structured and the Markovian environments for the photon and phonon modes as shown in Fig. 7. The structured environments are characterized by their spectral functions and the Markovian environments are characterized by their decay constants, which are obtained under the Weisskopf-Wigner approximation. In particular, the

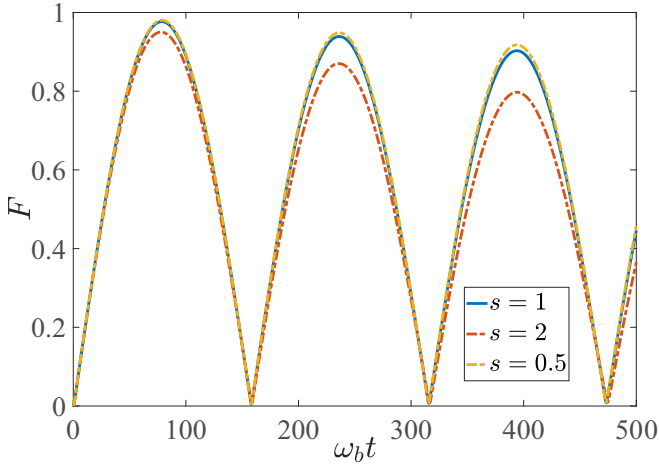


FIG. 8. The time evolution of the transfer fidelity under sub-Ohmic ($s < 1$), Ohmic ($s = 1$), and super-Ohmic ($s > 1$) environments for the photon mode and a fixed $1/f$ -noise environment for the phonon mode. The other parameters are set as $|\tilde{G}| = 0.02\omega_b$, $\eta = 1 \times 10^{-4}\omega_b$, $\omega_0 = 5\omega_b$, and $c = 1 \times 10^{-4}\omega_b$.

optical-mode decay rate is $\kappa_a = J_a(\omega_a)/2$ and the mechanical-mode decay rate is $\gamma_b = J_b(\omega_b)/2$. When both modes are embedded in the realistic structured environments (see the blue solid line), the conversion fidelity is close to 0.98 in the first period of Rabi oscillation and could be still maintained above 0.9 in the third period. It is nearly invariant when the environment for the phonon mode is changed to be a Markovian type (see the yellow dotted line). The conversion will be greatly damaged when the photon mode is subject to a Markovian type, and in this case, it is also insensitive to the choice of the phonon-mode environment (see the red dashed and purple dotted lines). In both cases, the conversion fidelity is no more than 0.35 and could not start a second period of Rabi oscillation. These results indicate that the non-Markovian noise from the structured environment for the photon mode are more significant than that for the phonon mode on protecting the conversion fidelity.

In Fig. 8, the phonon mode is subjected to a fixed $1/f$ noise with $k = -1$ and then one can observe the effects from the sub-Ohmic ($s = 0.5$), Ohmic ($s = 1$), and super-Ohmic ($s = 2$) environments for the photon mode on the time evolution of the transfer fidelity. We can see that the sub-Ohmic spectrum and the Ohmic spectrum are better than the super-Ohmic spectrum in terms of conversion fidelity. For the sub-Ohmic spectrum, the fidelity could be close to 0.99 during the first period of Rabi oscillation and still around 0.90 during the third period. These results are close to those for the Ohmic spectrum, while the fidelity will drop to about 0.80 during the third period of Rabi oscillation for the super-Ohmic spectrum.

In Fig. 9, one can observe that the conversion fidelity is also insensitive to different choices of the structured environments for the phonon mode. Under a fixed Ohmic environment for the photon mode, the conversion fidelity shows a slightly decreasing pattern with increasing $|k|$. Thus, in realistic situations, the conversion process between the photon mode and the phonon mode is strongly resilient to the $1/f$ -type noise for the phonon mode.

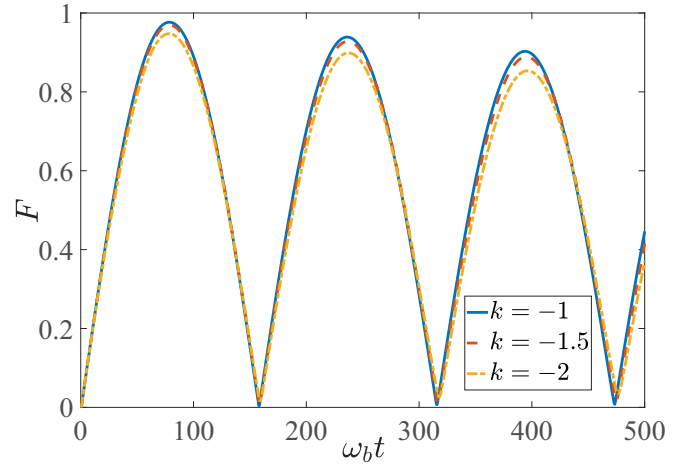


FIG. 9. The time evolution of the transfer fidelity under various environments for the phonon mode and a fixed structured environment for the photon mode with an Ohmic spectrum. The other parameters are set as $|\tilde{G}| = 0.02\omega_b$, $\eta = 1 \times 10^{-4}\omega_b$, $\omega_0 = 5\omega_b$, and $c = 1 \times 10^{-4}\omega_b$.

V. DISCUSSION AND CONCLUSION

When the yttrium iron garnet sphere are strongly pumped to generate a considerable number of magnons, the Kerr effect due to the ensued magnetocrystalline anisotropy could not be completely neglected. When the exciton number in the spin wave is much smaller than the total number of spins in YIG sphere, the system Hamiltonian in Eq. (1) can be modified to be [49,50]

$$\tilde{H}_S = H_S + Km^\dagger mm^\dagger m, \quad (37)$$

where K is the nonlinear coefficient for the Kerr effect. With the linear approximation, the Kerr term $Km^\dagger mm^\dagger m$ becomes $2K\langle m^\dagger m \rangle m^\dagger m$, and thus the Hamiltonian H_0 in Eq. (3) turns out to be

$$\tilde{H}_0 = \Delta_a a^\dagger a + \tilde{\Delta}_m m^\dagger m + \omega_b b^\dagger b, \quad (38)$$

where $\tilde{\Delta}_m \equiv \Delta_m + 2K\langle m^\dagger m \rangle$ [51]. Then the derivation process for the effective Hamiltonian describing the photon-phonon conversion [from Eq. (3) to Eq. (12)] would be merely revised in quantity to ensure that the frequency detuning of the magnon mode approaches the frequency of the cavity mode. The Kerr term will eventually only change the effective coupling strength \tilde{G} in Eq. (13). For a YIG sphere with a diameter about $250 \mu\text{m}$, the Kerr coefficient $K/2\pi \approx 6.4 \times 10^{-9} \text{ Hz}$ and the magnon exciton number $\langle m^\dagger m \rangle \approx 10^{14}$ corresponding to $G = Mg_{mb} \approx 10^7 \text{ Hz}$ via $M = \sqrt{\langle m^\dagger m \rangle}$. Then one can estimate that $K\langle m^\dagger m \rangle \approx 10^5 \text{ Hz}$, which is much smaller than Δ_m . It is therefore shown that our proposal also adapts to such a hybrid system even with a non-negligible Kerr effect.

In summary, we have presented a protocol to realize a photon-phonon conversion in a cavity magnomechanical system, where the magnon mode in the YIG sphere is coupled to both a microwave cavity mode and the mechanical-vibration mode in the same sphere. Our indirect photon-phonon conversion protocol has considerable merit in physics due to the strong controllability in this system. This magnon-assisted protocol relies on the effective Hamiltonian for coupling

photon and phonon, which is constructed in the strong-coupling regimes for both magnon-photon interaction and magnon-phonon interaction. We apply a bottom-up perturbation approach rather than the adiabatic-elimination technique, which is beneficial to shed light on more physics in special subspaces. In the open-system framework, the state fidelity of the photon-phonon conversion is mainly limited by the decay of the microwave cavity κ_a rather than the dissipation of the phonons γ_b , due to the fact that γ_b is much smaller than the phonon frequency ω_b [30]. We also analyze the effect from various environmental noises on the conversion fidelity using the non-Markovian Heisenberg-Langevin equations. Excellent results can be obtained when the cavity mode is under a structured environment with sub-Ohmic spectrum even if the phonons are in a Markovian environment. Our work in pursuit of the quantum state transfer and protection therefore provides

a different implementation of the photon-phonon interface realized in a solid system under realistic noises. It also extends the application of the cavity-magnomechanical system as a promising hybrid platform for quantum information processing.

ACKNOWLEDGMENTS

We acknowledge grant support from the National Science Foundation of China (Grants No. 11974311 and No. U1801661), Zhejiang Provincial Natural Science Foundation of China (Grant No. LD18A040001), and the Fundamental Research Funds for the Central Universities (Grant No. 2018QNA3004). We are thankful for the comments from an anonymous referee about the Zeeman interaction of microwave magnons and microwave photons.

-
- [1] D. Lachance-Quirion, Y. Tabuchi, A. Gloppe, K. Usami, and Y. Nakamura, *Appl. Phys. Express* **12**, 070101 (2019).
- [2] M. Elyasi, Y. M. Blanter, and G. E. W. Bauer, *Phys. Rev. B* **101**, 054402 (2020).
- [3] Y. Li, W. Zhang, V. Tyberkevych, W. K. Kwok, and V. Novosad, *J. Appl. Phys.* **128**, 130902 (2020).
- [4] C. A. Potts and J. P. Davis, *Appl. Phys. Lett.* **116**, 263503 (2020).
- [5] O. O. Soykal and M. E. Flatté, *Phys. Rev. Lett.* **104**, 077202 (2010).
- [6] O. O. Soykal and M. E. Flatté, *Phys. Rev. B* **82**, 104413 (2010).
- [7] H. Y. Yuan, P. Yan, S. Zheng, Q. Y. He, K. Xia, and M.-H. Yung, *Phys. Rev. Lett.* **124**, 053602 (2020).
- [8] Z.-X. Liu, H. Xiong, and Y. Wu, *Phys. Rev. B* **100**, 134421 (2019).
- [9] Y. Tabuchi, S. Ishino, T. Ishikawa, R. Yamazaki, K. Usami, and Y. Nakamura, *Phys. Rev. Lett.* **113**, 083603 (2014).
- [10] X. Zhang, C.-L. Zou, L. Jiang, and H. X. Tang, *Phys. Rev. Lett.* **113**, 156401 (2014).
- [11] M. Goryachev, W. G. Farr, D. L. Creedon, Y. Fan, M. Kostylev, and M. E. Tobar, *Phys. Rev. Appl.* **2**, 054002 (2014).
- [12] D. Lachance-Quirion, S. Piotr Wolski, Y. Tabuchi, S. Kono, K. Usami, and Y. Nakamura, *Science* **367**, 425 (2020).
- [13] Y. Tabuchi, S. Ishino, A. Noguchi, T. Ishikawa, R. Yamazaki, K. Usami, and Y. Nakamura, *Science* **349**, 405 (2015).
- [14] A. Wallraff, D. I. Schuster, A. Blais, L. Frunzio, and R.-S. Huang, *Nature (London)* **431**, 162 (2004).
- [15] X. Mi, J. V. Cady, D. M. Zajac, P. W. Deelman, and J. R. Petta, *Science* **355**, 156 (2017).
- [16] N. Samkharadze, G. Zheng, N. Kalhor, D. Brousse, A. Sammak, U. C. Mendes, A. Blais, G. Scappucci, and L. M. K. Vandersypen, *Science* **359**, 1123 (2018).
- [17] P. Forn-Díaz, J. Lisenfeld, D. Marcos, J. J. García-Ripoll, E. Solano, C. J. P. M. Harmans, and J. E. Mooij, *Phys. Rev. Lett.* **105**, 237001 (2010).
- [18] A. Ridolfo, S. Savasta, and M. J. Hartmann, *Phys. Rev. Lett.* **110**, 163601 (2013).
- [19] Y.-J. Zhao, Y.-L. Liu, Y.-X. Liu, and F. Nori, *Phys. Rev. A* **91**, 053820 (2015).
- [20] M. Aspelmeyer, T. J. Kippenberg, and F. Marquardt, *Rev. Mod. Phys.* **86**, 1391 (2014).
- [21] W.-Z. Zhang, J. Cheng, W.-D. Li, and L. Zhou, *Phys. Rev. A* **93**, 063853 (2016).
- [22] D. Vitali, S. Gigan, A. Ferreira, H. R. Böhm, P. Tombesi, A. Guerreiro, V. Vedral, A. Zeilinger, and M. Aspelmeyer, *Phys. Rev. Lett.* **98**, 030405 (2007).
- [23] T. A. Palomaki, J. D. Teufel, I. Marinković, and C. Lüschnauer, *Science* **342**, 710 (2013).
- [24] J. Cheng, X.-T. Liang, W.-Z. Zhang, and X. Duan, *Opt. Commun.* **430**, 385 (2019).
- [25] J. M. Raimond, M. Brune, and S. Haroche, *Rev. Mod. Phys.* **73**, 565 (2001).
- [26] Z.-L. Xiang, S. Ashhab, J. Q. You, and F. Nori, *Rev. Mod. Phys.* **85**, 623 (2013).
- [27] P. Forn-Díaz, L. Lamata, E. Rico, J. Kono, and E. Solano, *Rev. Mod. Phys.* **91**, 025005 (2019).
- [28] A. Reiserer and G. Rempe, *Rev. Mod. Phys.* **87**, 1379 (2015).
- [29] X. Zhang, C.-L. Zou, L. Jiang, and H. Tang, *Sci. Adv.* **2**, e1501286 (2016).
- [30] J. Li, S.-Y. Zhu, and G. S. Agarwal, *Phys. Rev. Lett.* **121**, 203601 (2018).
- [31] J. I. Cirac, P. Zoller, H. J. Kimble, and H. Mabuchi, *Phys. Rev. Lett.* **78**, 3221 (1997).
- [32] H. J. Kimble, *Nature (London)* **453**, 1023 (2008).
- [33] L. Tian and Z. Li, *Phys. Rev. A* **96**, 013808 (2017).
- [34] J. Zhang, K. Peng, and S. L. Braunstein, *Phys. Rev. A* **68**, 013808 (2003).
- [35] C. Genes, A. Mari, P. Tombesi, and D. Vitali, *Phys. Rev. A* **78**, 032316 (2008).
- [36] M. Schmidt, M. Ludwig, and F. Marquardt, *New J. Phys.* **14**, 125005 (2012).
- [37] V. Macrì, F. Nori, and A. F. Kockum, *Phys. Rev. A* **98**, 062327 (2018).
- [38] S.-f. Qi and J. Jing, *Phys. Rev. A* **101**, 033809 (2020).
- [39] L. Garziano, R. Stassi, V. Macrì, A. F. Kockum, S. Savasta, and F. Nori, *Phys. Rev. A* **92**, 063830 (2015).
- [40] S. A. Bender, A. Kamra, W. Belzig, and R. A. Duine, *Phys. Rev. Lett.* **122**, 187701 (2019).

- [41] G. D. de Moraes Neto, F. M. Andrade, V. Montenegro, and S. Bose, *Phys. Rev. A* **93**, 062339 (2016).
- [42] S. Singh, H. Jing, E. M. Wright, and P. Meystre, *Phys. Rev. A* **86**, 021801(R) (2012).
- [43] A. Vochezer, T. Kampschulte, K. Hammerer, and P. Treutlein, *Phys. Rev. Lett.* **120**, 073602 (2018).
- [44] X. Xu, Z. Zhang, and Z. Liang, *Phys. Rev. A* **100**, 053616 (2019).
- [45] M. Christandl, N. Datta, A. Ekert, and A. J. Landahl, *Phys. Rev. Lett.* **92**, 187902 (2004).
- [46] K. W. Chang and C. K. Law, *Phys. Rev. A* **81**, 052105 (2010).
- [47] A. J. Leggett, S. Chakravarty, A. T. Dorsey, M. P. A. Fisher, A. Garg, and W. Zwerger, *Rev. Mod. Phys.* **59**, 1 (1987).
- [48] S. GröBlacher, A. Trubarov, N. Prigge, G. D. Cole, M. Aspelmeyer, and J. Eisert, *Nat. Commun.* **6**, 7606 (2015).
- [49] Y.-P. Wang, G.-Q. Zhang, D. Zhang, T.-F. Li, C.-M. Hu, and J. Q. You, *Phys. Rev. Lett.* **120**, 057202 (2018).
- [50] Y.-P. Wang, G.-Q. Zhang, D. Zhang, X.-Q. Luo, W. Xiong, S.-P. Wang, T.-F. Li, C.-M. Hu, and J. Q. You, *Phys. Rev. B* **94**, 224410 (2016).
- [51] G.-Q. Zhang, Y.-P. Wang, and J. Q. You, *Sci. China Phys. Mech. Astron.* **62**, 987511 (2019).